


Article

Continuous and Intermittent Planetary Ball Milling Effects on the Alloying of a Bismuth Antimony Telluride Powder Mixture

Georgios Samourganidis *  and Theodora Kyratsi

Department of Mechanical and Manufacturing Engineering, University of Cyprus, Nicosia 1678, Cyprus

* Correspondence: samourganidis.georgios@ucy.ac.cy

Abstract: This study investigates the effects of continuous and in-steps mechanical alloying of a bismuth antimony telluride powder mixture ($\text{Bi}_{0.4}\text{Sb}_{1.6}\text{Te}_{3.0}$) via the mechanical planetary ball milling (PBM) process as a function of milling time and powder mixture amount. X-ray diffraction (XRD) and scanning electron microscopy (SEM) were used to characterize the phase, composition, and morphology of the alloy. The alloyed powder with the optimum PBM conditions was then hot pressed (HP), and its thermoelectric properties were further investigated. The results on the alloying of the powder mixture showed that due to the high agglomeration tendency of BST during the PBM process, a significant deviation occurs in the development of a single-phase state over time when the powder mixture is milled continuously and in-steps. 'In-steps' refers to the procedure of interrupting the PBM process and detaching the agglomerated powder adhering to the inner walls of the vessel. This task was repeated every hour and a half of the PBM process for a total of 12 h, and the results were compared with those of the 12 h continuous PBM process of the same mixture. In addition, the procedure was repeated with different amounts of mixture (100 g and 150 g) to determine the most efficient method of producing the material as a function of time. As for the thermoelectric profile of the powder, the data showed results in direct agreement with those in the literature.

Keywords: mechanical alloying; planetary ball milling; bismuth antimony telluride; thermoelectric materials



Citation: Samourganidis, G.; Kyratsi, T. Continuous and Intermittent Planetary Ball Milling Effects on the Alloying of a Bismuth Antimony Telluride Powder Mixture. *Inorganics* **2023**, *11*, 221. <https://doi.org/10.3390/inorganics11050221>

Academic Editors: Roberto Nisticò, Torben R. Jensen, Luciano Carlos, Hicham Idriss and Eleonora Aneggi

Received: 20 April 2023

Revised: 15 May 2023

Accepted: 16 May 2023

Published: 20 May 2023



Copyright: © 2023 by the authors. Licensee MDPI, Basel, Switzerland. This article is an open access article distributed under the terms and conditions of the Creative Commons Attribution (CC BY) license (<https://creativecommons.org/licenses/by/4.0/>).

1. Introduction

Over the last two decades, there has been an increasing trend in the study and development of thermoelectric (TE) alloys from submicron- and nano-powders, necessitating the incorporation of mechanical alloying (MA) processes in the field of TE materials. However, the race to create fine and ultra-fine TE material powders using MA started a little earlier [1–4]. In general, the MA process is based on the repetitive process of cold welding and fracturing of powder particles with the rotational kinetic energy of the grinding balls [5]. It is a high-energy process capable of producing alloys that would be impossible to create otherwise, with a typical example being the aluminum–tantalum alloy (Al-Ta), for which the melting method for the alloy's formation becomes restrictive due to the large difference in the melting points of its individual elements (Aluminum at 933 K, Tantalum at 3293 K) [6].

One of the most commonly used MA methods is that of the planetary ball milling (PBM) process [7–11], and it has significant advantages over other conventional methods (mixer mills, stirred mills, etc.). It is effective for wet and dry grinding processes due to the high mechanical stresses reached during the operation, and submicron and nano-sized particles can be achieved with the proper milling balls and milling conditions. The operating principle of this method is based on the rotation of the grinding containers around the common axis of rotation of the main disk (also known as the sun-disk), as well as the vertical axis of rotation of the containers themselves. In this manner, the kinetic energy of the grinding containers, due to rotation and self-rotation, is greatly increased, resulting in

high impact energies of the milling balls inside, which in turn crash any powder particles trapped on their surface in between collisions [12–15]. The PBM process is most effective when the milling conditions, such as rotational speed, milling time, ball-to-material ratio, number, size, and material of the grinding balls, are first evaluated [16,17]. In particular, the material of the milling balls should be chosen based on the reactions that occur during the milling process in order to avoid any side effects that could contaminate or change the structure of the grinding mixture. The materials from which grinding balls are usually made of are tungsten carbide (WC), corundum (Al_2O_3), stainless steel (SS), zirconia (ZrO_2), and agate (SiO_2) [18–22].

As previously stated, the introduction of MA in the world of TE materials accelerated the development of new thermoelectric alloys with higher efficiencies and wider temperature ranges [23,24]. The current state of TE materials shows conversion efficiencies ranging from 5% to 20%, a percentage range that can be improved further using suitable methods of alloying, doping, and nanostructuring. The efficiency of a TE material is projected through the dimensionless thermoelectric figure of merit, ZT , which is directly related to the physical properties of the material and is calculated from the relationship $ZT = S^2 * \sigma / \kappa$, where S is the Seebeck coefficient, σ the electrical conductivity, and κ the thermal conductivity. In the case of an ideal TE material (high Seebeck coefficient and electrical conductivity, low thermal conductivity), the ZT value should be greater than one in order for it to have an efficiency greater than 10% [25–29]. One of the most widely studied and commercialized TE alloys are those of bismuth telluride due to their excellent performance in the temperature range [250 K–400 K] [30–37]. These alloys are easily prepared as fine powders by MA, and their thermoelectric properties are acquired through mechanical and thermal treatments [38,39].

The current study looks into the manufacturing process of a specific bismuth telluride TE alloy, that of $\text{Bi}_{0.4}\text{Sb}_{1.6}\text{Te}_{3.0}$, in two distinct but related ways. This particular p-type alloy possess superior TE performance around room temperature [37], making it a frequently researched and used bismuth telluride alloy. Although the methods used are presented only for the production of the specific material, they can be applied to the general group of TE materials that tend to agglomerate during the alloying process using the MA methods. From an innovation standpoint, this work demonstrates manufacturing techniques that can process materials faster and more efficiently, using less time and energy while producing larger quantities. For example, with the ongoing research in additive manufacturing and 3D printing of TE materials [40–42], the need for cost-effective and efficient methods to produce TE powder materials in large quantities becomes critical.

2. Experimental Procedures

As starting materials, elemental powders of Bi (99.99% metal basis, –200 mesh), Sb (99.5% metal basis, –200 mesh), and Te (99.5% metal basis, –200 mesh) were used and weighed according to the desired stoichiometry. To avoid oxidation phenomena and to protect the user against the toxicity of the materials, the whole procedure (weighing process, powder loading, and unloading) was carried out in a glovebox containing argon. The powder mixture with the correct composition was then loaded into a 250 mL tungsten carbide (WC) vial along with 110 WC milling balls with a diameter of $d = 10$ mm and milled in an argon atmosphere using the FRITSCH planetary mono mill Pulverisette 6 classic line. All experiments were performed under the same PBM conditions: milling speed at 400 rpm, 10 min of milling time per repetition, and 5 min of pause time per repetition. The reverse mode was always ON during the milling process, as it favors the alloying process of dry materials and improves the homogeneity of the mixture. As the PBM process in this study was performed for two different amounts of material mixture, the ball-to-material ratio varied in each test. In particular, the ratio was 8.6:1 for the 100 g of powder mixture (BST-100) and 5.7:1 for the 150 g of powder mixture (BST-150).

The X-ray diffraction patterns of the powder were acquired using a Rigaku MiniFlex diffractometer, and the structural and phase characteristics were analyzed using the X-Pert

highscore plus software program. All X-ray diffraction graphs were taken in the angular range of 10–60 degrees, angular step of 0.02 degree, and scan speed of 1 degree per minute. The acceleration voltage was set to 30 kV and the beam current to 15 mA, resulting in Cu-K α radiation ($k = 1.5406 \text{ \AA}$). The chemical composition (EDX) and morphology (SEM) of the powder was examined with the use of TESCAN VEGA-II Model LSH scanning electron microscopy, and the EDX analysis was carried out under identical conditions (magnification, live time, dead time, takeoff angle, etc.) for different regions of the powder sample.

To investigate the thermoelectric properties of the alloy powder under optimal milling time and amount conditions, a small portion of it was HP inside a cylindrical graphite matrix, using a Thermal Technology Graphite Hot Press (Model HP20-4560), to form a 10 mm diameter and 2.5 mm thick disk pellet. The HP conditions were optimal and were based on our previous work [34]. Specifically, the alloy powder was HP for 1 h at the temperature of 420 °C under a mechanical press of 80 MPa (pressure equivalent to 640 kg). The temperature ramp rate was set to 10 °C/min, and the pressing ramp rate was set to 16 kg/min. The average density of the HP sample was $\rho_{sample} = 6.022 \text{ g/cm}^3$ when measured using the Archimedes method in ethanol, which is greater than 90% of the bulk material ($\rho_{bulk} = 6.564 \text{ g/cm}^3$ as measured experimentally). The thermoelectric evaluation of the HP sample was performed in the temperature range [300 K–500 K] using a Netzsch LFA 457 laser flash apparatus (thermal properties) and a ZEM-3 series ULVAC-Riko system (electrical properties).

3. Results and Discussion

Figure 1 shows the X-ray diffraction patterns versus time of the BST-150 powder mixture PBMed in-steps. The time step here was 1.5 h, for a total of 12 h, and in between steps, the milling container was removed from the milling machine and placed inside an argon-filled glovebox, where the agglomerated powder was extracted, milled with agate mortar, sieved, and then added back to the PBM process (Figure 2). The agate mortar grinding and sieving sub-process was repeated until no powder was left on the sieving basket and all agglomerated powder particles were thoroughly ground. The vertical axis of the intensities is linearly scaled. The alloying process of the elements is clearly visible from the behavior of the BST's base peak (015) (shown in the JCPDS plot). As the milling time increases, the multi-phase material degrades into a single-phase material.

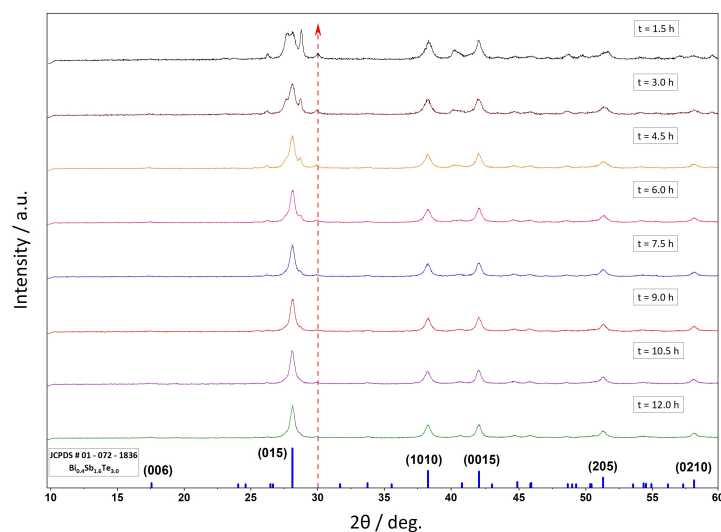


Figure 1. X-ray diffraction patterns of the BST-150 mixture versus time for each step of the PBM process.

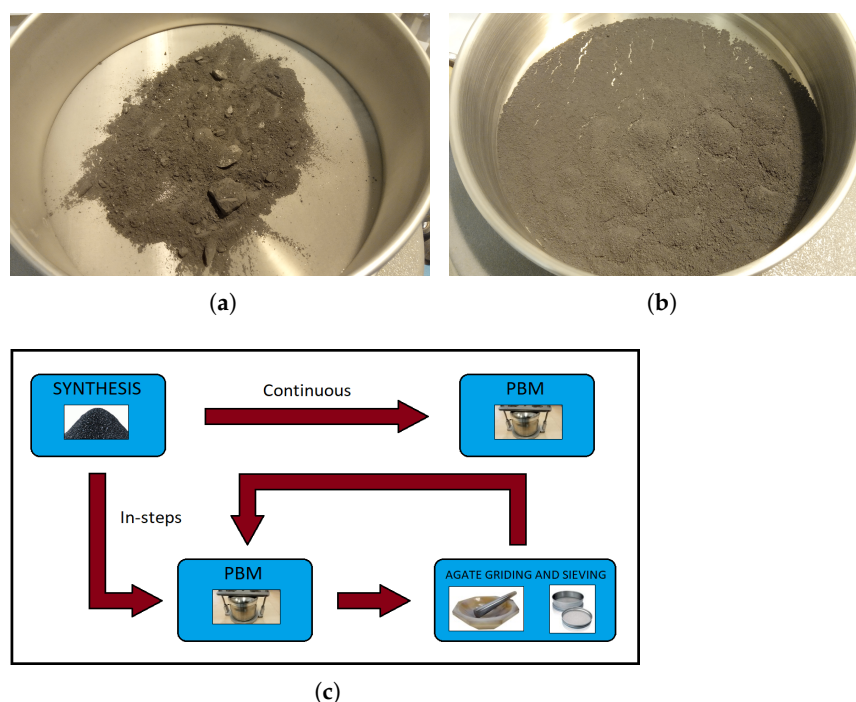


Figure 2. Agglomerated powder (a) before and (b) after agate grinding and sieving; (c) milling process diagram for the two distinct methods.

The red dashed line represents the tellurium (Te) powder characteristic peak (Figure 3), which was observed to have the lowest damping rate during the milling steps, indicating tellurium's difficulty in participating in the alloying process. This can be attributed to the higher diffusion rate that tellurium has compared to the other two elements within the agglomerated powder as a result of its entrapment there, without participating in the alloying process at the same rate. At this point, it should be noted that the mechanical ball milling method alloys two or more materials during the collision of the milling balls with each other or with the walls of the milling container. The kinetic energy of the balls is converted into heat at the point of impact, instantly welding together the powder particles present. Thus, in cases where the grinding powder has a tendency to agglomerate on the base of the milling container, it traps a large percentage of the individual chemical elements, which can no longer participate in the alloying process because they never come into contact with the milling balls.

Figure 3 presents the X-ray diffraction pattern of the BST-150 powder mixture PBMed for 24 h in-steps, as well as the X-ray diffraction patterns of its individual elemental powders and the JCPDS diagram. According to the 24 h X-ray diffraction pattern, the characteristic tellurium peak appears to have completely faded, compared to the 12 h plot (Figure 1), and is now at the noise level. This signifies that the concentration of the elemental tellurium in the mixture has decreased significantly, with the majority of it now alloyed with the other elements.

Figure 4 shows the X-ray diffraction pattern of the BST-150 powder mixture for the two different PBM methods, continuous and in-steps, and clearly demonstrates the entrapment mechanism of the individual chemical elements in the agglomerated powder described above. The upper X-ray diffraction pattern shows the PBM process with steps for a total milling time of 3 h; the middle shows the continuous PBM process for a total milling time of 12 h; and the bottom shows the PBM process with steps for a total milling time of 12 h. The main characteristic peak (015) of the BST in the first two plots indicates that the mixture is still elemental and multiphase, and by comparing them, it is possible to conclude that after 3 h of continuous PBM, the mixture inside the vial has already agglomerated, significantly reducing the alloying process. Furthermore, when comparing the 12 h plots, it is clear

that the alloying process is much more effective when the milling process is carried out in-steps. However, as previously discussed, the single-phase state for the BST-150 mixture occurs after 24 h of the PBM process in-steps because the characteristic of the tellurium peak (shown with the dashed line) fades completely at that point.

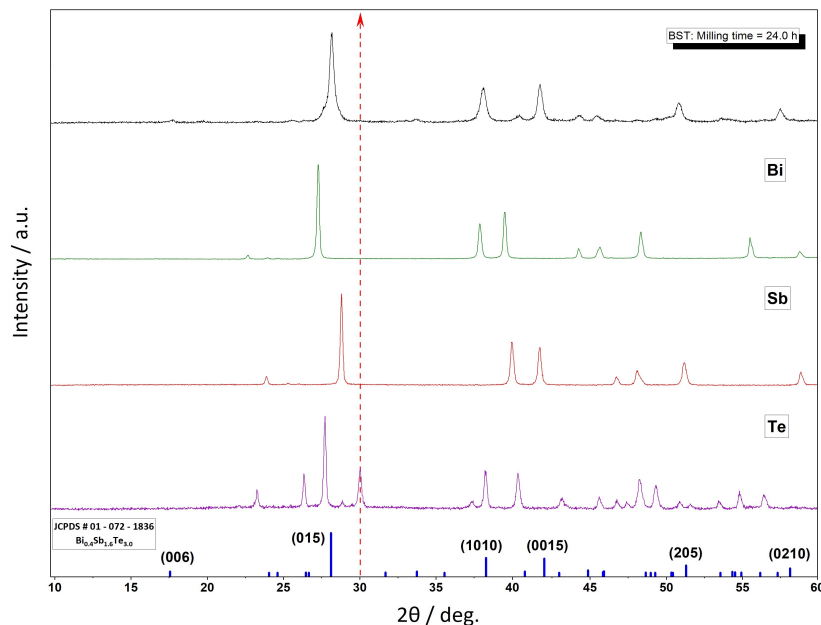


Figure 3. X-ray diffraction pattern of the BST-150 mixture milled in-steps for 24 h, along with the corresponding JCPDS diagram. For comparison, X-ray diffraction patterns of the individual elemental powders are also shown.

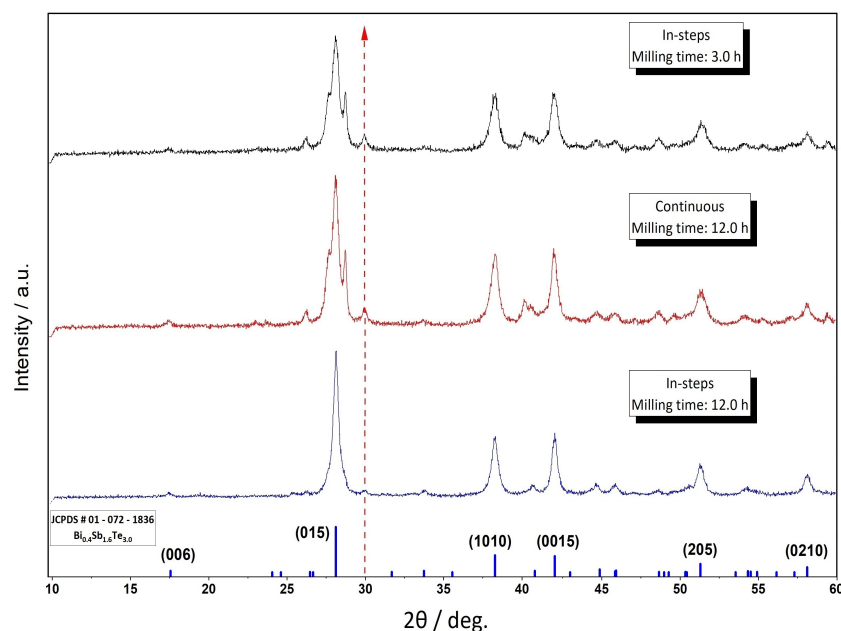


Figure 4. Comparison X-ray diffraction patterns for the BST-150 powder.

The procedures for the BST-100 powder mixture were the same as those for the BST-150. The X-ray diffraction patterns versus time of the BST-100 powder mixture PBMed in-steps and the X-ray diffraction pattern of the same mixture PBMed for 12 h in-steps, along with the X-ray diffraction patterns of its individual elemental powders and the JCPDS diagram, are shown in Figures 5 and 6, respectively. For convenience, the X-ray diffraction patterns in Figure 6 are presented every 3 h. The alloying process is faster in the case of the BST-100

powder mixture because of the larger ball-to-material ratio. In particular, when comparing the 3 h of PBM for the BST-150 and BST-100 powder mixtures, the main characteristic peak of the BST appears to have reconstructed to a smooth peak for the latter. Additionally, in the case of the 12 h PBM, the characteristic peak of the tellurium powder has faded completely for the BST-100 powder mixture, compared to the BST-150 where the same peak fades within 24 h of PBM. Based on these comparison results, it is feasible to conclude that reducing the powder mixture quantity by 50% (and thus increasing the ball-to-material ratio) reduces the optimum milling time for the alloying process by a factor of two.

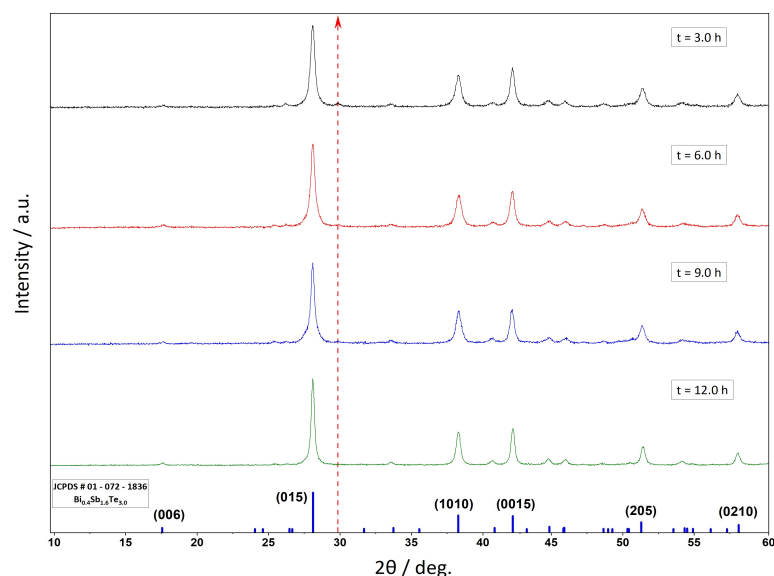


Figure 5. X-ray diffraction patterns of the BST-100 powder mixture versus time for each step of the PBM process.

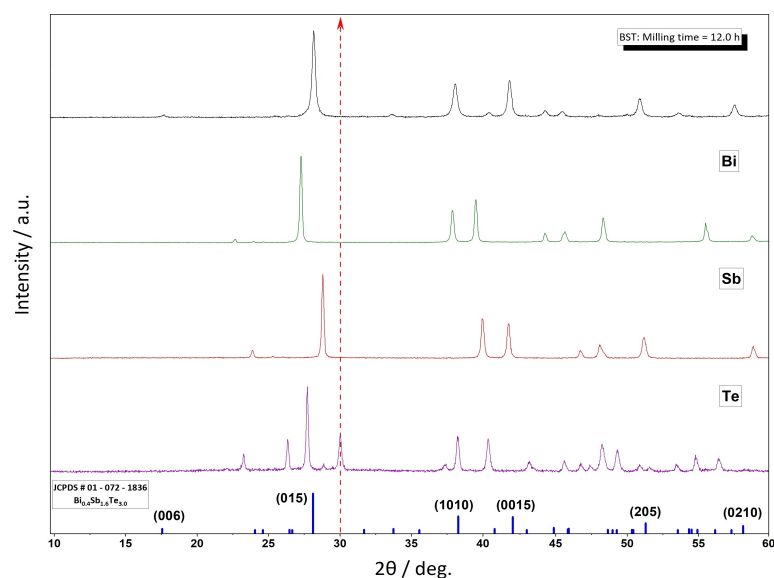


Figure 6. X-ray diffraction pattern of the BST-100 powder milled in-steps for 12 h, along with the corresponding JCPDS diagram. For comparison, X-ray diffraction patterns of the individual elemental powders are also shown.

Shown in Figure 7 is the X-ray diffraction patterns of the BST-100 powder mixture for the two different PBM processes. The upper X-ray diffraction pattern shows the PBM process with steps for a total milling time of 3 h, the middle shows the continuous PBM process for a total milling time of 12 h, and the bottom shows the PBM process with steps for a total milling time of 12 h. When the bottom graph is compared to the middle one, it is clear that the multiphase state is still strongly present in the mixture and comparable to the first graph. This can also be seen in the shape of the BST's base characteristic peak (015) in the middle graph, which is depicted with a red circle in both the graph and the inset, as an extra peak coming up on the side of the main peak.

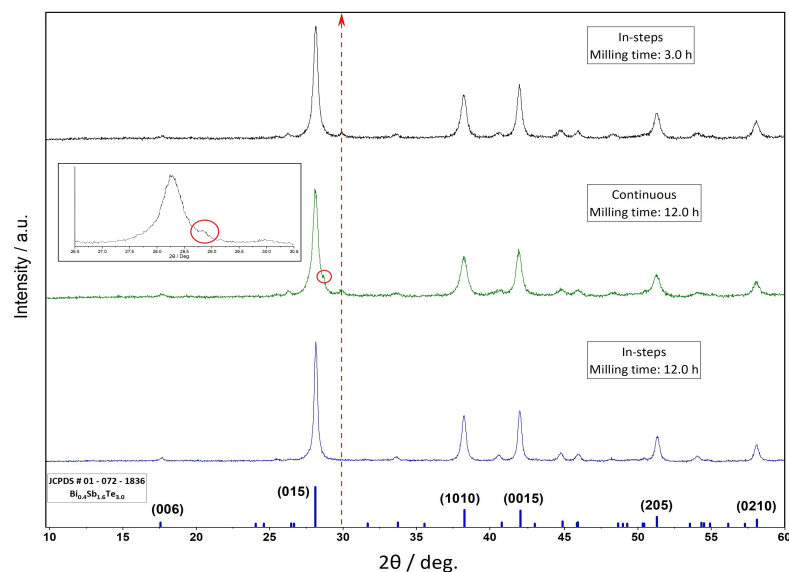


Figure 7. Comparison of X-ray diffraction patterns for the BST-100 powder.

The chemical composition and powder morphology of the produced BST powder with the optimum PBM conditions were determined using the SEM/EDS characterization method. Figure 8 presents the results of the SEM/EDS analysis for the BST-100 powder mixture, which was also the same for the BST-150 powder mixture. In terms of powder morphology, Figure 8a shows the image from the secondary electron detector (SE), where the majority of the particles appear to be smaller than 5 μm in size and have an irregular shape and geometry. Figure 8b shows the image from the back-scattered electron detector (BSE). The contrast of the image is uniformly spread here, implying no secondary phases in the powder mixture and agreeing with the X-ray diffraction results presented above. Finally, the chemical composition of the produced alloy can be seen qualitatively and quantitatively from the energy-dispersive X-ray spectroscopy (EDS) analysis shown in Figure 8c. All three elements are clearly present in the alloy, with their radiated energies and percent atomic values listed in the inset. It should be noted at this point that this analysis was performed on a large agglomerated particle of the alloy in order to avoid radiation from the carbon tape substrate on which the powder was placed.

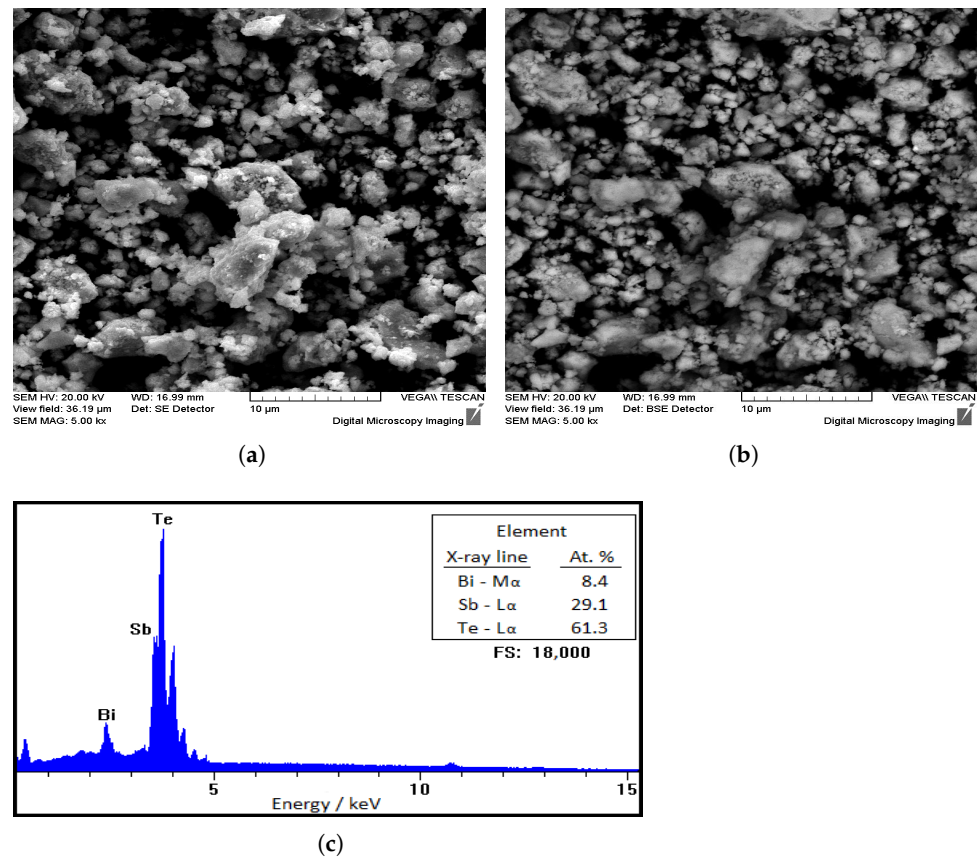


Figure 8. Scanning electron microscopy images: (a) SE detector, (b) BSE detector, (c) EDS spectrum.

As previously stated in Section 2, a small portion of the produced BST powder was hot pressed under optimal pressing and temperature conditions, yielding a cylindrical disk pellet with a thickness of $t_h = 2.5$ mm and a diameter of $d = 10$ mm, the thermoelectric properties of which are shown in Figure 9 along with the results of the studies [36,37]. All measurements and calculations were performed in the temperature range of [300 K–500 K]. Starting with the property of thermal conductivity κ , as shown in Figure 9a, its values vary within the range of [0.7–1.1] $\text{Wm}^{-1}\text{K}^{-1}$ and have an overall minimum value of $\kappa_{min} = 0.73 \text{ Wm}^{-1}\text{K}^{-1}$ in the temperature range of [325 K–350 K], which is the lowest when compared to the other two studies. Similarly, the Seebeck coefficient S (Figure 9b) exhibits an overall maximum over the same temperature range, with its maximum value at $S_{max} = 260 \mu\text{V K}^{-1}$, followed by a steady rapid decline. In comparison to the other two studies, the Seebeck coefficient in this work is higher within the temperature range of [300 K–375 K]. The electrical conductivity σ , on the other hand (Figure 9c), has an overall minimum of $\sigma_{min} = 2.52 \times 10^4 \text{ S/m}$ in the temperature range of [450 K–475 K], which results from a steep decline and is the lowest value when compared to the other two studies. The power factor of the sample is calculated by combining the values of the Seebeck coefficient and electrical conductivity using the equation $\text{PF} = S^2\sigma$, and as shown by the curve in Figure 9d, there is a constant drop as a function of temperature with no maxima or minima, which is consistent with the other two studies. Finally, the figure of merit ZT is shown in Figure 9e and was calculated using the equation $ZT = \text{PF}/\kappa$. As can be seen from the curve, a total maximum with a value of $ZT = 1.02$ appears at the temperature of $T = 325$ K, and represents the thermoelectric material's optimal performance temperature. In comparison to the other two studies, the ZT appears to be very close to the curves as they move across a zone as a whole.

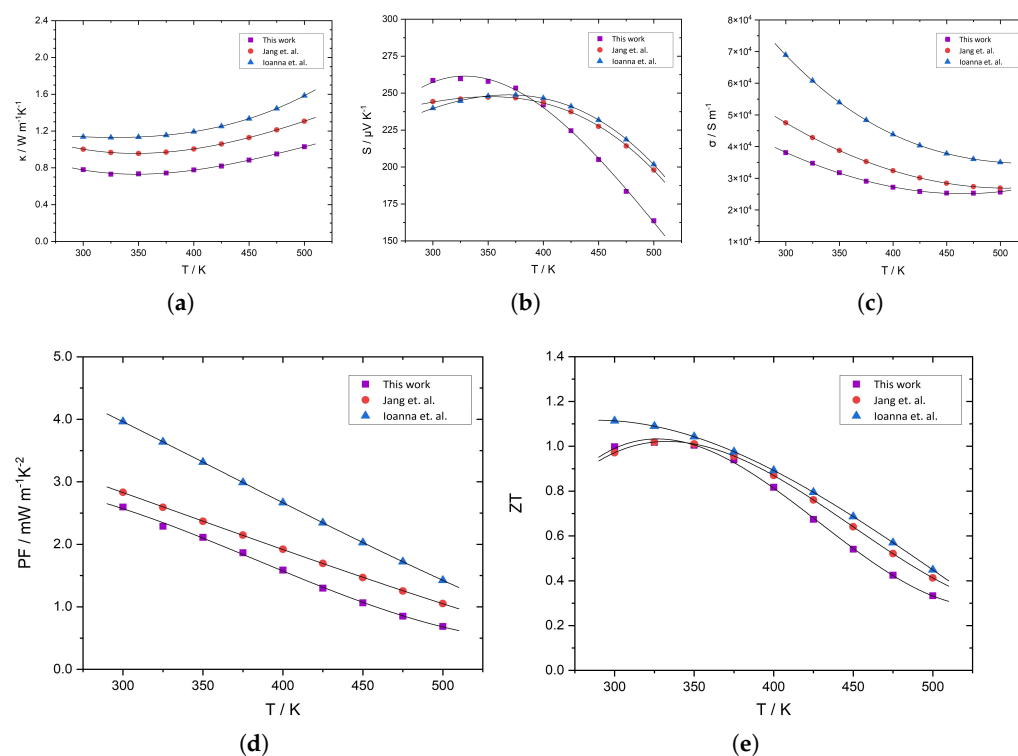


Figure 9. Thermoelectric properties of the produced BST powder compared to the literature (Jang et al. [36] and Ioannou et al. [37]): (a) Thermal conductivity, (b) Seebeck coefficient, (c) Electrical conductivity, (d) Power factor, and (e) Figure of merit.

4. Conclusions

The impact of both continuous and intermittent planetary ball milling on the alloying of the bismuth antimony telluride ($\text{Bi}_{0.4}\text{Sb}_{1.6}\text{Te}_{3.0}$) thermoelectric material is discussed in the current work. Because of the mixture's high agglomeration tendency, the results revealed a significant difference in the alloying process in terms of milling time and powder mixture quantity, when the powder mixture was PBMed in-steps versus continuously. The term “in-steps” refers to the procedure in which the PBM process is interrupted and the agglomerated powder adhering to the inner walls of the container is detached, ground in an agate mortar, and sieved before the alloying process is resumed. In particular, the results showed that PB Ming the mixture continuously for more than 3 h has no effect on the alloying process because most of the elemental compounds are already trapped inside the agglomerated powder and do not participate in the alloying process. Additionally, applying the same procedure for two different amounts of powder mixture (100 g and 150 g) showed that increasing the powder mixture amount by 50% *w/w* resulted in an increase in the overall time needed to achieve the single-phase condition of the alloy by a factor of 2. Concerning the thermoelectric properties of the produced powder, the results revealed a very good thermoelectric profile, consistent with the literature, with the figure of merit reaching a maximum value of $Z = 1.02$ at $T = 325$ K, demonstrating the effectiveness of the presented technique to process materials faster and more efficiently, consuming less time and energy while producing larger quantities.

Author Contributions: Conceptualization, G.S.; methodology, G.S.; software, G.S.; validation G.S.; formal analysis, G.S. and T.K.; investigation, G.S.; resources, T.K.; data curation, G.S.; writing—original draft preparation, G.S.; writing—review and editing, G.S. and T.K.; visualization, G.S.; supervision, T.K.; project administration, T.K.; funding acquisition, T.K. All authors have read and agreed to the published version of the manuscript.

Funding: This work was funded by the University of Cyprus (internal project ADD-THERM).

Institutional Review Board Statement: Not applicable.

Informed Consent Statement: Not applicable.

Data Availability Statement: Data available on request from the authors.

Conflicts of Interest: The authors declare no conflicts of interest.

References

1. Hasezaki, K.; Nishimura, M.; Umata, M.; Tsukuda, H.; Araoka, M. Mechanical alloying of BiTe and BiSbTe thermoelectric materials. *Mater. Trans. JIM* **1994**, *35*, 428–432. [[CrossRef](#)]
2. Wunderlich, W.; Pixius, K.; Schilz, J. Microstructure of mechanical alloyed Si₇₆Ge_{23.95}P_{0.05}. *Nanostruct. Mater.* **1995**, *6*, 441–444. [[CrossRef](#)]
3. Tokiai, T.; Uesugi, T.; Eton, Y.; Tamura, S.; Yoneyama, Y.; Koumoto, K. Thermoelectric properties of p-type bismuth telluride material fabricated by plasma sintering of metal powder mixture. *J. Ceram. Soc. Jpn.* **1996**, *104*, 837–843. [[CrossRef](#)]
4. Sugiyama, A.; Kobayashi, K.; Ozaki, K.; Nishio, T.; Matsumoto, A. Preparation of functionally graded Mg₂Si-FeSi₂ thermoelectric material by mechanical alloying-pulsed current sintering process. *Nippon Kinzoku Gakkaishi (1952)* **1998**, *62*, 1082–1087.
5. Suryanarayana, C. Mechanical alloying and milling. *Prog. Mater. Sci.* **2001**, *46*, 1–184. [[CrossRef](#)]
6. El-Eskandarany, M.S. *Mechanical Alloying: For Fabrication of Advanced Engineering Materials*; William Andrew: Norwich, NY, USA, 2001.
7. Burmeister, C.F.; Kwade, A. Process engineering with planetary ball mills. *Chem. Soc. Rev.* **2013**, *42*, 7660–7667. [[CrossRef](#)]
8. Zheng, Y.; Liu, C.; Miao, L.; Lin, H.; Gao, J.; Wang, X.; Chen, J.; Wu, S.; Li, X.; Cai, H. Cost effective synthesis of p-type Zn-doped MgAgSb by planetary ball-milling with enhanced thermoelectric properties. *RSC Adv.* **2018**, *8*, 35353–35359. [[CrossRef](#)]
9. Bumrungpon, M.; Hirota, K.; Takagi, K.; Hanasaku, K.; Hirai, T.; Morioka, I.; Yasufuku, R.; Kitamura, M.; Hasezaki, K. Synthesis and thermoelectric properties of bismuth antimony telluride thermoelectric materials fabricated at various ball-milling speeds with yttria-stabilized zirconia ceramic vessel and balls. *Ceram. Int.* **2020**, *46*, 13869–13876. [[CrossRef](#)]
10. Balasubramanian, P.; Battabyal, M.; Bose, A.C.; Gopalan, R. Effect of ball-milling on the phase formation and enhanced thermoelectric properties in zinc antimonides. *Mater. Sci. Eng. B* **2021**, *271*, 115274. [[CrossRef](#)]
11. Im, H.J.; Koo, B.; Kim, M.S.; Lee, J.E. Optimization of high-energy ball milling process for uniform p-type Bi-Sb-Te thermoelectric material powder. *Korean J. Chem. Eng.* **2022**, *39*, 1227–1231. [[CrossRef](#)]
12. Fokina, E.; Budim, N.; Kochnev, V.; Chernik, G. Planetary mills of periodic and continuous action. *J. Mater. Sci.* **2004**, *39*, 5217–5221. [[CrossRef](#)]
13. Mio, H.; Kano, J.; Saito, F.; Kaneko, K. Optimum revolution and rotational directions and their speeds in planetary ball milling. *Int. J. Miner. Process.* **2004**, *74*, S85–S92. [[CrossRef](#)]
14. Bruckmann, A.; Krebs, A.; Bolm, C. Organocatalytic reactions: Effects of ball milling, microwave and ultrasound irradiation. *Green Chem.* **2008**, *10*, 1131–1141. [[CrossRef](#)]
15. Stolle, A.; Szuppa, T.; Leonhardt, S.E.; Ondruschka, B. Ball milling in organic synthesis: Solutions and challenges. *Chem. Soc. Rev.* **2011**, *40*, 2317–2329. [[CrossRef](#)]
16. Schneider, F.; Stolle, A.; Ondruschka, B.; Hopf, H. The Suzuki-Miyaura reaction under mechanochemical conditions. *Org. Process. Res. Dev.* **2009**, *13*, 44–48. [[CrossRef](#)]
17. Szuppa, T.; Stolle, A.; Ondruschka, B.; Hopfe, W. Solvent-free dehydrogenation of γ -terpinene in a ball mill: Investigation of reaction parameters. *Green Chem.* **2010**, *12*, 1288–1294. [[CrossRef](#)]
18. Sasaki, K.; Masuda, T.; Ishida, H.; Mitsuda, T. Structural degradation of tobermorite during vibratory milling. *J. Am. Ceram. Soc.* **1996**, *79*, 1569–1574. [[CrossRef](#)]
19. Balema, V.P.; Wiench, J.W.; Pruski, M.; Pecharsky, V.K. Solvent-free mechanochemical synthesis of phosphonium salts. *Chem. Commun.* **2002**, *7*, 724–725. [[CrossRef](#)]
20. Rodríguez, B.; Bruckmann, A.; Bolm, C. A highly efficient asymmetric organocatalytic aldol reaction in a ball mill. *Chem.–Eur. J.* **2007**, *13*, 4710–4722. [[CrossRef](#)]
21. Patil, P.R.; Kartha, K.R. Solvent-free synthesis of thioglycosides by ball milling. *Green Chem.* **2009**, *11*, 953–956. [[CrossRef](#)]
22. Tadier, S.; Le Bolay, N.; Rey, C.; Combes, C. Co-grinding significance for calcium carbonate–calcium phosphate mixed cement. Part I: Effect of particle size and mixing on solid phase reactivity. *Acta Biomater.* **2011**, *7*, 1817–1826. [[CrossRef](#)] [[PubMed](#)]
23. Gayner, C.; Kar, K.K. Recent advances in thermoelectric materials. *Prog. Mater. Sci.* **2016**, *83*, 330–382. [[CrossRef](#)]
24. Liu, W.; Hu, J.; Zhang, S.; Deng, M.; Han, C.G.; Liu, Y. New trends, strategies and opportunities in thermoelectric materials: A perspective. *Mater. Today Phys.* **2017**, *1*, 50–60. [[CrossRef](#)]
25. Chasmar, R.; Stratton, R. The thermoelectric figure of merit and its relation to thermoelectric generators. *Int. J. Electron.* **1959**, *7*, 52–72. [[CrossRef](#)]
26. Rowe, D.; Min, G. Evaluation of thermoelectric modules for power generation. *J. Power Sources* **1998**, *73*, 193–198. [[CrossRef](#)]
27. Rowe, D.M. *CRC Handbook of Thermoelectrics: Macro to Nano*; CRC Taylor & Francis: Boca Raton, FL, USA, 2006.
28. Ismail, B.I.; Ahmed, W.H. Thermoelectric power generation using waste-heat energy as an alternative green technology. *Recent Patents Electr. Electron. Eng. (Former. Recent Patents Electr. Eng.)* **2009**, *2*, 27–39. [[CrossRef](#)]

29. Fleurial, J.P. Thermoelectric power generation materials: Technology and application opportunities. *JOM* **2009**, *61*, 79–85. [[CrossRef](#)]
30. Yamashita, O.; Tomiyoshi, S.; Makita, K. Bismuth telluride compounds with high thermoelectric figures of merit. *J. Appl. Phys.* **2003**, *93*, 368–374. [[CrossRef](#)]
31. Hong, S.J.; Chun, B.S. Microstructure and thermoelectric properties of extruded n-type 95% Bi₂Te₂–5% Bi₂Se₃ alloy along bar length. *Mater. Sci. Eng. A* **2003**, *356*, 345–351. [[CrossRef](#)]
32. Chung, D.Y.; Hogan, T.P.; Rocci-Lane, M.; Brazis, P.; Ireland, J.R.; Kannewurf, C.R.; Bastea, M.; Uher, C.; Kanatzidis, M.G. A new thermoelectric material: CsBi₄Te₆. *J. Am. Chem. Soc.* **2004**, *126*, 6414–6428. [[CrossRef](#)]
33. Kanatzia, A.; Papageorgiou, C.; Lioutas, C.; Kyratsi, T. Design of ball-milling experiments on Bi₂Te₃ thermoelectric material. *J. Electron. Mater.* **2013**, *42*, 1652–1660. [[CrossRef](#)]
34. Symeou, E.; Nicolaou, C.; Delimitis, A.; Androulakis, J.; Kyratsi, T.; Giapintzakis, J. High thermoelectric performance of Bi_{2-x}Sb_xTe₃ bulk alloys prepared from non-nanostructured starting powders. *J. Solid State Chem.* **2019**, *270*, 388–397. [[CrossRef](#)]
35. Symeou, E.; Nicolaou, C.; Kyratsi, T.; Giapintzakis, J. Enhanced thermoelectric properties in vacuum-annealed Bi_{0.5}Sb₁Te₃ thin films fabricated using pulsed laser deposition. *J. Appl. Phys.* **2019**, *125*, 215308. [[CrossRef](#)]
36. Jang, K.W.; Kim, H.J.; Jung, W.J.; Kim, I.H. Charge transport and thermoelectric properties of p-type Bi_{2-x}Sb_xTe₃ prepared by mechanical alloying and hot pressing. *Korean J. Met. Mater.* **2018**, *56*, 66–71.
37. Ioannou, I.; Ioannou, P.S.; Kyratsi, T.; Giapintzakis, J. Low-cost preparation of highly-efficient thermoelectric Bi_xSb₂Te₃ nanostructured powders via mechanical alloying. *J. Solid State Chem.* **2023**, *319*, 123823. [[CrossRef](#)]
38. Zakeri, M.; Allahkarami, M.; Kavei, G.; Khanmohammadian, A.; Rahimpour, M. Synthesis of nanocrystalline Bi₂Te₃ via mechanical alloying. *J. Mater. Process. Technol.* **2009**, *209*, 96–101. [[CrossRef](#)]
39. Jimenez, S.; Perez, J.G.; Tritt, T.M.; Zhu, S.; Sosa-Sanchez, J.L.; Martinez-Juarez, J.; López, O. Synthesis and thermoelectric performance of a p-type Bi_{0.4}Sb_{1.6}Te₃ material developed via mechanical alloying. *Energy Convers. Manag.* **2014**, *87*, 868–873. [[CrossRef](#)]
40. Shi, J.; Chen, H.; Jia, S.; Wang, W. 3D printing fabrication of porous bismuth antimony telluride and study of the thermoelectric properties. *J. Manuf. Process.* **2019**, *37*, 370–375. [[CrossRef](#)]
41. Yan, Y.; Ke, H.; Yang, J.; Uher, C.; Tang, X. Fabrication and thermoelectric properties of n-type CoSb_{2.85}Te_{0.15} using selective laser melting. *ACS Appl. Mater. Interfaces* **2018**, *10*, 13669–13674. [[CrossRef](#)]
42. Qiu, J.; Yan, Y.; Luo, T.; Tang, K.; Yao, L.; Zhang, J.; Zhang, M.; Su, X.; Tan, G.; Xie, H.; et al. 3D Printing of highly textured bulk thermoelectric materials: Mechanically robust BiSbTe alloys with superior performance. *Energy Environ. Sci.* **2019**, *12*, 3106–3117. [[CrossRef](#)]

Disclaimer/Publisher’s Note: The statements, opinions and data contained in all publications are solely those of the individual author(s) and contributor(s) and not of MDPI and/or the editor(s). MDPI and/or the editor(s) disclaim responsibility for any injury to people or property resulting from any ideas, methods, instructions or products referred to in the content.